ISSN 0023-1584, Kinetics and Catalysis, 2007, Vol. 48, No. 6, pp. 789–793. © MAIK "Nauka/Interperiodica" (Russia), 2007.
Original Russian Text © N.V. Kolesnichenko, L.E. Kitaev, Z.M. Bukina, N.A. Markova, V.V. Yushchenko, O.V. Yashina, G.I. Lin, A.Ya. Rozovskii, 2007, published in Kinetika i Kataliz, 2007, Vol. 48, No. 6, pp. 846–850.

Synthesis of Gasoline from Syngas via Dimethyl Ether

N. V. Kolesnichenko[a], L. E. Kitaev[b], Z. M. Bukina[a], N. A. Markova[a], V. V. Yushchenko[b], O. V. Yashina[a], G. I. Lin[a], and A. Ya. Rozovskii[a]

[a] *Topchiev Institute of Petrochemical Synthesis, Russian Academy of Sciences, Moscow, 117912 Russia*
[b] *Department of Chemistry, Moscow State University, Moscow, 119992 Russia*
e-mail: yashina@ips.ac.ru

Received February 28, 2006

Abstract—Zeolite H-TsVM has been loaded with palladium by different methods. The properties of the resulting catalysts in gasoline synthesis from syngas via dimethyl ether depend on the way in which palladium was introduced. The catalysts have been characterized by ammonia temperature-programmed desorption (TPD), temperature-programmed reaction with hydrogen, and X-ray photoelectron spectroscopy. According to ammonia TPD data, use of a palladium ammine complex instead of palladium chloride reduces the concentration of strong acid sites and raises the concentration of medium-strength acid sites, thereby reducing the yield of C_1–C_4 hydrocarbons and increasing the yield of gasoline hydrocarbons. At T = 340°C, P = 100 atm, and GHSV = 2000 h^{-1}, the dimethyl ether conversion is 98–99%, the gasoline selectivity is >60%, the isoparaffin content of the product is ~61%, and the arene content is not higher than 29%.

DOI: 10.1134/S0023158407060043

The challenge of oil depletion and the steady rise of gasoline prices orientate mankind towards synthetic fuels, posing the problem of converting natural gas or coal into motor fuel.

There are two commercial processes for obtaining gasoline from syngas, namely Sasol (Fischer–Tropsch method) and Mobil (via methanol). The products resulting from these processes are qualitatively different. The Sasol product includes considerable amounts of oxygen-containing derivatives and olefins. The Mobil product is dominated by aromatic and branched aliphatic hydrocarbons belonging to the gasoline fraction [1]. Accordingly, the gasoline resulting from this process has a high octane number of 90–95 and needs no enhancement. As compared to Sasol gasoline, it has a higher quality and is obtained in higher yield. Furthermore, there is no need to remove the oxygen-containing compounds from the product mixture resulting from the Mobil process.

The Mobil process is based on a well-proven technology for obtaining methanol from syngas and additionally includes methanol conversion into gasoline hydrocarbons. Approximately 80% of the overall cost of the process is due to syngas production and syngas conversion into methanol. As a consequence, the Mobil gasoline is rather expensive. An intermediate product in the conversion of methanol into hydrocarbons is dimethyl ether (DME).

A more promising method is to use, instead of methanol, DME obtained from syngas by direct synthesis. This process is more efficient than the process involving methanol synthesis. Furthermore, the DME conversion product contains less water, implying lower power consumption at the stage of gasoline separation from the aqueous fraction. For the first time, the synthesis of antiknock gasoline from DME was carried out in the late 1970s [2–4]. Later, new processes for antiknock gasoline production from syngas via DME were developed on the basis of DME synthesis from CO, CO_2, and H_2 [5–7]. The catalyst used in this technology is zeolite ZSM-5 combined with various oxides [8].

We demonstrated that the high-silica zeolite H-TsVM containing Pd and zinc oxide (Pd–ZnO–TsVM) is an active catalyst for DME conversion into hydrocarbons [9]. However, this catalyst shows an insufficiently high gasoline selectivity because of the inappropriate way of introducing palladium. In view of this, we studied how the physicochemical properties of the Pd–ZnO–TsVM catalyst and its catalytic properties in DME conversion depend on the nature of the palladium precursor.

EXPERIMENTAL

In the synthesis of high-octane hydrocarbons from CO and H_2 via DME, we used a catalyst consisting of a high-silica (Si/Al = 15) zeolite in H-form (H-TsVM, Russia) and palladium and zinc compounds. Catalyst samples were obtained by mixing the zeolite with γ-Al_2O_3 (30 wt %) and impregnating the mixture with aqueous solutions of zinc chloride and palladium chloride. The catalysts were calcined in air at 500°C for 4 h and were then reduced in flowing hydrogen at 380°C for 3 h. According to IR spectroscopic data (KBr technique), the zeolite in the catalysts retained its original structure.

Table 1. Catalytic properties of Pd–H-TsVM–ZnO in DME conversion

Sample	DME conversion, wt %			Composition of the liquid phase, wt %			
	total	into gas	into gasoline	isoparaffins	*n*-paraffins	cycloparaffins	aromatic hydrocarbons
Cat 1	98–99	60.3	39.7	54.0	4.1	11.0	30.9
Cat 2	98–99	39.0	61.0	60.8	6.0	4.5	28.7

Note: $T = 340°C$, $P = 10$ MPa, GHSV = 2000 h^{-1}.

We examined two catalysts loaded with palladium in different ways (Cat 1 and Cat 2). In the case of Cat 1, palladium was introduced from an aqueous hydrochloric acid solution; in the case of Cat 2, as ammine complexes from aqueous ammonia.

X-ray photoelectron spectra (XPS) were recorded on a PHI 5500 ESCA spectrometer (Physical Electronics). Photoemission was excited with AlK_α ($h\nu$ = 1486.6 eV) or MgK_α ($h\nu$ = 1253.6 eV) radiation of 300 W power. The residual gas pressure in the analysis chamber was 6–8 × 10^{-10} Torr. The atomic concentrations of elements were derived from survey scans using relative sensitivity factors and the PC ACCESS ESCA V7.2c program package. High-resolution spectra were recorded at a pass energy of 58.70 eV and an energy step size of 0.25 eV. The high-resolution spectra were processed by linear least squares fitting to the Gauss and Lorentz functions.

The analysis depth for the tape on which the specimen was mounted was varied by argon ion sputtering. The ion energy was 2 keV, and the argon partial pressure was 15 mPa, affording a sputtering rate of about 25 Å/min. Ion sputtering reduced the carbon content from 7–8 to 1 at %, which corresponds to the hydrocarbon level in the analysis chamber. According to the literature, the Zn 2*p* and Pd 3*d* binding energies (eV) for the metals and their compounds introduced into the catalysts are as follows [10]: Zn^0 1021.8–1021.9; ZnO, 1021.8–1022.5; $ZnCl_2$ 1021.9–1023.1; Pd^0 335.1–335.3; PdO, 336.3; $PdCl_2$ 337.8.

Temperature programmed reactions (TPR) with hydrogen were carried out as follows. The sample (0.1 g) was heated to 450°C within 1 h in flowing argon, held at 450°C for 1 h, and cooled to room temperature in flowing argon. Next, the reactor was switched to an argon–hydrogen mixture (3.5 vol % H_2) and the heating of the sample was monitored. The sample was held in the argon–hydrogen mixture at room temperature for 40 min, and the temperature was then raised at a constant rate of ~8 K/min while monitoring the hydrogen uptake chromatographically.

In order to acquire ammonia temperature programmed desorption (TPD) data, the sample (0.1 g) was calcined at 500°C for 4 h in flowing dry air and for 1 h in flowing helium at the same temperature, was cooled to room temperature, and was treated with a flowing nitrogen–ammonia (1 : 1 vol/vol) mixture for 30 min. Next, the loosely bound ammonia was flushed off the sample for 1 h at 100°C, the sample was cooled to room temperature, and programmed heating at a rate of 8 K/min was begun. Heating was continued until all of the adsorbate was removed from the sample. This was indicated by the restoration of the base line. In all experiments, the gas flow rate was 0.5 cm^3/s. The gases were purified and dried before the experiments.

Ammonia TPD data were processed by fitting the experimental curve to the calculated curve [11]. This method enabled us to find the total acidity, to determine the distribution of acid sites over the ammonia desorption activation energy between its minimum (E_{min}) and maximum (E_{max}), and to calculate the average activation energy $\langle E \rangle$ (which characterizes the average acidity of the sites) for the entire desorption interval. The activation energy range was divided into equal intervals of 5 kJ/mol. For each interval, the sites were assumed to be homogeneous and their acidity was assumed to be determined by the average activation energy corresponding to the middle of the interval.

The catalysts were tested at $P = 10$ MPa in a high-pressure flow system (designed at the Topchiev Institute of Petrochemical Synthesis, Russian Academy of Sciences) consisting of two reactors placed in series, one for DME synthesis and the other for DME conversion into gasoline. The vapor–gas mixture flowing from the DME synthesis reactor into the gasoline synthesis reactor contained the following components (mol %): DME, 13; N_2, 15; CO, 24; CO_2, 15; H_2, 33. The compositions of the gaseous and liquid products were determined chromatographically.

In order to see how the product composition varies as the catalyst operates, we tested catalyst samples in a flow microreactor, making on-line mass spectrometric analyses of the products (catalyst sample size of 0.5–0.7 cm^3, atmospheric pressure, T = 300–360°C, DME (10 vol %) + He mixture, GHSV = 1000–2000 h^{-1}).

RESULTS AND DISCUSSION

The results of the testing of the catalysts Cat 1 and Cat 2 in the high-pressure flow system are presented in Table 1.

It is clear from Table 1 that gasoline hydrocarbon selectivity depends strongly on the palladium introduction method. The selectivity of Cat 2 is 1.5 times as high

Table 2. Elemental composition of the surface layer of the catalysts from XPS data

Sample	Sputtering time, min	C	N	O	Zn	Si	Al	Pd	Cl
Cat 1	0	7.64	0.37	59.03	0.17	7.76	24.23	0.17	0.51
	5	0.98	–	61.79	0.26	8.87	27.44	0.24	0.42
Cat 2	0	8.31	0.39	59.70	0.67	13.40	16.82	0.27	0.44
	5	1.01	0.14	61.41	0.75	13.82	21.95	0.40	0.53

as the selectivity of Cat 1 owing to the lower yield of the gaseous (C_1–C_4) products. The composition of the liquid hydrocarbon phase is nearly the same for these catalysts.

Both Cat 1 and Cat 2 were also tested in the flow microreactor at 340–360°C at atmospheric pressure, and the products were quantified by on-line mass spectrometric analysis. This technique allowed us to estimate the variation of the product composition during catalyst operation.

For both Cat 1 and Cat 2 at 340°C, the DME conversion at the early stages of the reaction (in the first 15 min) is close to 100% and the product consists largely of ethylene and a small amount of ethane (2–3 wt %). CO_2 and water were also detected in the product mixture.

As the reaction proceeds further, the proportion of the C_2 hydrocarbons falls dramatically and the products forming over Cat 1 and Cat 2 become different. Methane, C_3 and C_4 hydrocarbons, and lower aromatic compounds appear in the products obtained with Cat 1. Under the same conditions, the product obtained with the catalyst prepared using the ammonia method (Cat 2) consists mainly of aliphatic C_4–C_6 hydrocarbons and contains five-membered cyclic hydrocarbons. As the temperature is raised to 360°C, products of further conversion appear. These are aromatic C_7 and C_8 hydrocarbons in the case of Cat 1 and C_6 and C_7 arenes in the case of Cat 2. The CO_2 concentration increases in both cases. As the temperature is decreased to 300°C, the DME conversion decreases sharply and methanol appears in the product mixture.

The states of the elements in the surface layers of the catalyst pellets calcined in air at 500°C for 6 h were judged from XPS data. Below, we present the binding energies for the metal compounds present in the catalysts, as well as the relative contributions from these compounds (in parentheses) determined by separating the XPS peaks into components.

For Cat 1 before sputtering, the Pd 3*d* spectrum consists of lines at 336.11 eV (73%, PdO) and 337.83 eV (27%, $PdCl_2$); for the same sample sputtered for 5 min, 336.30 eV (73%, PdO) and 337.80 eV (27%, $PdCl_2$). The Zn 2*p* spectrum before sputtering is 1022.05 eV; the same spectrum after 5-min-long sputtering is 1022.35 eV.

For Cat 2 before sputtering, the Pd 3*d* spectrum is 336.07 eV (85%, PdO) and 337.66 eV (15%, $PdCl_2$); for the same sample sputtered for 5 min, 336.20 eV (85%, PdO) and 337.90 eV (15%, $PdCl_2$). The Zn 2*p* spectrum before sputtering is 1022.35 eV; the same spectrum after 5-min-long sputtering is 1022.35 eV.

The Pd 3*d* spectrum can unambiguously be separated into peaks due to palladium oxide and palladium chloride. Evidently, palladium oxide is the dominant phase in both catalysts. Its percentage is higher in the catalyst loaded with palladium using an aqueous ammonia solution (Cat 2); therefore, $PdCl_2$ in this sample is more readily oxidizable during calcination. The Zn 2*p* spectrum consists of a single peak. We believe that this peak is mainly due to $ZnCl_2$. It is remarkable that the argon ion sputtering of the samples exerted no effect on the palladium oxide and chloride percentages.

Table 2 lists atomic concentrations in the surface layers of the samples before and after argon ion sputtering.

Note that the Si/Al ratio (at %) reflects the state of the catalyst surface, not of the zeolite surface, since the catalyst contains alumina as the support. Note also that, as compared to Cat 1, Cat 2 has a substantially higher surface concentration of zinc atoms. The chlorine concentration is proportionally higher in Cat 2, indicating that the catalyst contains $ZnCl_2$ rather than zinc oxide.

In order to gain information concerning the state of the supported metal particles capable of absorbing, or reacting with, hydrogen, we used the hydrogen TPR method. We found that the primary temperature jump is 11.1°C for Cat 1 and 6.0°C for Cat 2. The TPR curve for Cat 1 shows peaks at 96, 425, 796, and 970°C (Fig. 1). The total hydrogen uptake for this sample is 63.9 μmol/g. A more complicated TPR spectrum was observed for Cat 2. As this sample was heated in hydrogen, its TPR curve exhibited minima at 79 and 125°C due to hydrogen desorption (Fig. 1). As compared to the TPR curve of Cat 1, the TPR curve of Cat 2 shows a stronger hydrogen absorption peak (516°C), which has two high-temperature shoulders at ~610 and ~720°C.

These distinctions can arise from the difference between the metal particle sizes on the surfaces of the oxide matrices. The findings that the interaction between Cat 1 and hydrogen is more exothermic and that the TPR curve of this sample shows several peaks in a wide temperature range indicate that the supported

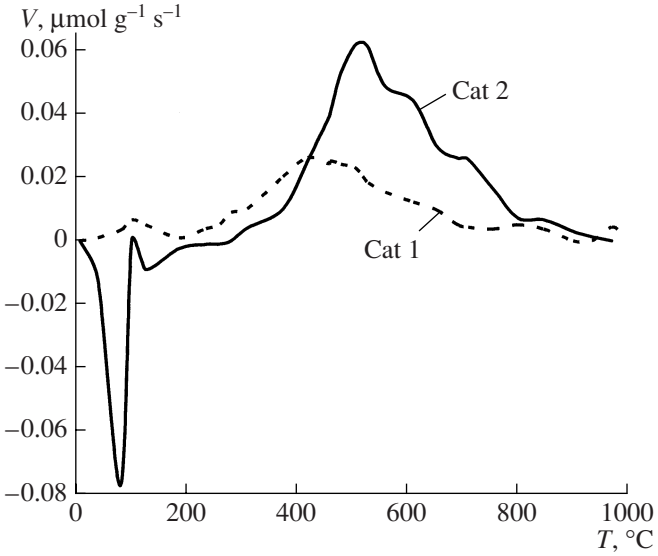

Fig. 1. Hydrogen TPR spectrum of the zeolite-containing catalysts Cat 1 and Cat 2.

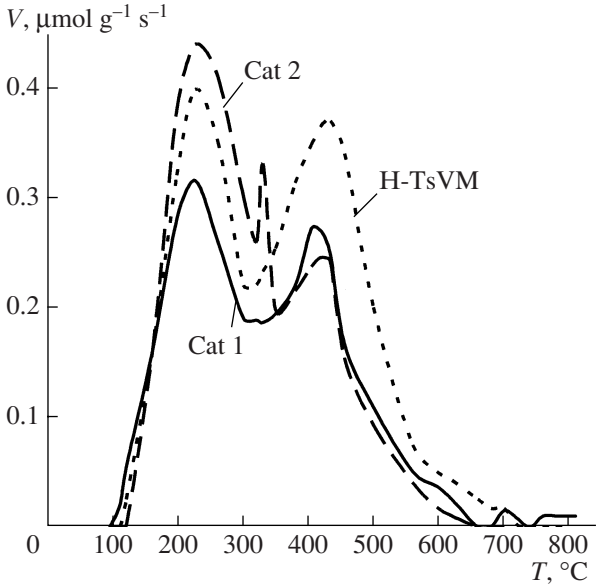

Fig. 2. Ammonia TPD spectra of zeolite H-TsVM and the zeolite-containing catalysts Cat 1 and Cat 2.

palladium particles are energetically rather heterogeneous and this heterogeneity is manifested in their interaction with hydrogen. The energetic heterogeneity can arise from the broad particle-size distribution [12, 13]. In the case of Cat 2, there is a single peak, which is more intensive. This suggests that the palladium particles in Cat 2 are energetically more homogeneous. Furthermore, this sample desorbs part of the absorbed hydrogen upon heating.

The acid properties of zeolite H-TsVM, Cat 1, and Cat 2 were studied by ammonia TPD (Fig. 2).

The NH_3 TPD curve of the starting zeolite H-TsVM shows two well-defined peaks, one in the low-temperature region and the other in the high-temperature region. The TPD curves of both catalysts are similar to the TPD curve of the zeolite, but the curve of Cat 2 has a narrow peak between the low- and high-temperature peaks. The extra peak is likely not associated with ammonia adsorption on acid sites. Considering that the palladium ion can bind a nonstoichiometric number of ammonia molecules, it can be assumed that this peak arises from the formation and decomposition of $Pd(NH_3)_x^{2+}$ ions. Apparently, similar nonstoichiometric binding takes place in hydrogen TPR in the case of Cat 2, which desorbs hydrogen at comparatively low temperatures.

Table 3. Acid site distribution over the activation energy of ammonia desorption (E_d, kJ/mol)

Sample	Total molar amount of acid sites, μmol/g	$E_d < 95$	$95 \le E_d < 130$	$E_d > 130$
H-TsVM	873	6	311	556
Cat 1	640	11	258	371
Cat 2	641*	15	337	289

* This value is the difference between the molar amount of potential sites according to ammonia TPD data (721 μmol/g) and the amount of ammonia bound as palladium complexes (80 μmol/g).

The formation of the ammine complexes can be viewed as a specific manifestation of the "catalytic memory" effect. Indeed, Cat 2 was prepared by impregnating the support with an aqueous ammonia solution of a palladium salt. The resulting complexes were decomposed by calcination in air and by reduction in flowing hydrogen. The new structures thus obtained "remember" their precursors and can reproduce themselves as the catalyst is treated with hydrogen in the TPR experiment or with ammonia in the TPD experiment.

The molar amounts of adsorption sites and the activation energies of desorption for the solids examined are listed in Table 3. Taking into account the temperature ranges of the peaks, for the sake of more convenient data analysis, the acidity spectra can be divided into three activation energy regions: $E_d < 95$ kJ/mol (weak sites), 95 kJ/mol $< E_d <$ 130 kJ/mol (medium-strength sites), and $E_d > 130$ kJ/mol (strong sites).

Comparing the catalysts in terms of acid sites readily demonstrates that pure H-TsVM has the largest number of acid sites and the largest proportion of strong acid sites. The introduction of alumina and the palladium and zinc compounds reduces the number of strong acid sites; however, for Cat 2, these components cause a buildup of medium strength sites (95 kJ/mol $\le E_d <$ 130 kJ/mol). Note that the decomposition of the palladium ammine complex (indicated by the middle

Table 4. Intervals of activation energy of ammonia desorption (kJ/mol) according to TPD data

Sample	$E_{d,\,min}$	$E_{d,\,max}$	$\langle E_d \rangle$
H-TsVM	96	189	146
Cat 1	92	189	141
Cat 2	97	178	137

peak in the TPD curve) for Cat 2 corresponds to the acid site strength region of $E_d > 130$ kJ/mol.

Furthermore, an analysis of the $E_{d,\,min}$ and $E_{d,\,max}$ data and the average activation energies of ammonia desorption (Table 4) shows that the strength of the acid sites decreases on passing from the pure zeolite to the catalysts, particularly Cat 2.

The data presented in Tables 1 and 3 suggest that a decrease in the concentration of strong acid sites and an increase in the concentration of medium-strength acid sites, observed on passing from Cat 1 to Cat 2, reduce the yield of C_1–C_4 hydrocarbons and favor the formation of gasoline hydrocarbons.

It can be assumed that Cat 1, which has a higher concentration of strong acid sites (according to ammonia TPD data), is a stronger adsorbent of ethylene, a primary product of DME conversion [14]. The main conversion route of this tightly bound species is cracking, as is indicated by the presence of methane in the product mixture and by the formation of condensation products. The formation of five-membered cyclic hydrocarbons, which are coke precursors, in the gas phase over Cat 2 is evidence of suppressed coking.

REFERENCES

1. Mills, G.A., *Chem.-Tech.*, 1977, vol. 7, no. 7, p. 418.
2. US Patent 3894102, 1975.
3. US Patent 4011275, 1977.
4. USSR Inventor's Certificate 632296, *Byull. Izobret.*, 1978, no. 41.
5. US Patent 5459166, 1995.
6. RF Patent 2143417, *Byull. Izobret.*, 1999, no. 12.
7. Thomson, R., Montes, C., Davis, M.E., and Wolf, E.E., *J. Catal.*, 1990, vol. 124, p. 401.
8. Stocker, M., *Microporous Mesoporous Mater.*, 1999, vol. 29, p. 3.
9. RF Patent 2248341, 2005.
10. Moulder, J.F., Stickle, W.F., Sobol, P.E., and Bomben, K.D., in *Handbook of X-ray Photoelectron Spectroscopy*, Chastain, J., Ed., Eden Prairie, Minn.: Perkin Elmer, 1992.
11. Yushchenko, V.V., *Zh. Fiz. Khim.*, 1997, vol. 71, no. 4, p. 628.
12. Matyi, R.J., Schwartz, L.H., and Butt, J.B., *Catal. Rev. Sci. Eng.*, 1987, vol. 29, no. 2, p. 49.
13. Chernavskii, P.A., Kiselev, V.V., Murav'eva, G.P., and Pankina, G.V., *Zh. Fiz. Khim.*, 1994, vol. 68, no. 7, p. 1288.
14. Shaikhutdinov, Sh.K., Baumer, M., and Freund, H.-J., *21st Symp. on Fundamental Catalysis and Surface Science*, Limerick, Ireland, 2001.